19th Brazilian Congress of Thermal Sciences and Engineering
November 6th–10th, 2022, Bento Gonçalves - RS - Brazil

# ENC-2022-0612
# POWER-LAW FLUID FLOW BEHAVIOR ON POROUS MEDIA INTERFACE

**Bresolin, C. S.**
**Fiorot, G. H.**
Universidade Federal do Rio Grande do Sul
Departamento de Engenharia Mecânica
cirilo.bresolin@ufrgs.br
guilherme.fiorot@ufrgs.br

**Minussi, R. B.**
Universidade Federal do Paraná
Campus Pontal - Centro de Estudos do Mar
robertaminussi@ufpr.br

***Abstract.*** *Non-Newtonian fluid flows conjugated with porous media occur in many industrial and natural processes. How the fluid rheological and porous material characteristics affect the flow still needs more understating. In this manuscript, a power-law fluid flow in a channel half filled with a porous matrix is simulated using the Lattice Boltzmann Method. Is observed how the fluid index and pore diameter influence the Darcian velocity, the fluid strain-rate at the interface, and the gain of discharge. The results show that immediately after the porous interface there is a momentum gain of a hundredfold. The hydraulic resistance is greater for a fluid index smaller than 1.0. The conditions at the interface are function from the pore diameter, and the discharge gain is greater for shear-thinning fluids for the same Darcian flow*

***Keywords:*** *Power-law fluids, Rheology, Porous Media, Interface*

## 1. INTRODUCTION

Non-Newtonian fluid flows through a porous media occur in natural phenomena and industrial processes such as enhanced oil recovery (EOR), filtration, hemodynamics, and soil remediation, among others. Commonly, these processes present an interface between the porous matrix and the free flow. A problem post is how the porous interface affects the flow dynamics. Given that macroscopic models for the free flow would require a set of boundary conditions to be solved, such an interface should be modeled properly to take into consideration the effects of the porous matrix without the need of solving the mesoscopic or even microscopic problem.

In this scenario, the classical interface boundary condition proposed by Beavers and Joseph (1967) arises as a simple solution, establishing the shear rate at the interface between free flow and porous flow as a function of the Darcian velocity and porous medium properties. This, however, could be rather simplistic and not be able to represent the complexity of non-Newtonian fluid flows, even though it has already been proven to be useful for some flow configurations (Sengupta and De, 2019; Fiorot and Maciel, 2019; Cloete and Smit, 2012). Models such as Bars and Worster (2006) studied even more complex phenomena at the interface during solidification processes and propose a viscous transition zone to account for the fluid-fluid viscous effects near the wall. Considering more complex fluids, Cloete and Smit (2012) developed an analytical solution for a Herschel-Bulkley laminar flow over a porous surface showing that good agreement can be found with analytical solutions and numerical simulations. In the same line of work, Sengupta and De (2019) propose an analytical solution for a Bingham fluid flow over a porous layer for a closed channel, while Fiorot and Maciel (2019) proposed a similar analysis using Beavers and Joseph (1967) boundary condition for an open-channel flow of a Herschel-Bulkley fluid.

Then, it is clear that, although simple boundary conditions can have a certain utility, the identification of a proper relationship between flow properties at the interface is crucial for proper flow modeling.

To study the interface without the inherent simplifications of analytical models as well as the volume averaging techniques for the Brinkman-Navier-Stokes Equations, a numerical simulation is set up to solve the velocity field using the

Lattice Boltzmann Method employing two-relaxation-time collision operator model (TRT) (d'Humières and Ginzburg, 2009). The literature has shown a wide range of non-Newtonian fluid flow and complex geometries using the LBM (Aharonov and Rothman, 1993; Rakotomalala *et al.*, 1996; Sullivan *et al.*, 2006), showing that it can be a useful tool for practical applications. A 2D laminar Poiseuille flow of a power-law fluid is numerically solved through a channel half filled with a porous matrix thus allowing the identification of the exact geometrical interface between free flow and porous flow. The purpose of the present paper is to study how the porous media and fluid rheological parameters affect the fluid-porous interface phenomena. Properties at the interface between the porous medium and the free flow fluid are explored to study possible influences of fluid rheology on classical relationships.

## 2. METHODOLOGY

The LBM is a numerical scheme to solve the space and time parts of the Boltzmann Transport Equation. The discretization of the transport equation generates a set of discrete particle populations $f_i$, that follow the given evolution equation,

$$f_i(\vec{r}+\vec{e}_i, t+1) - f_i(\vec{r}, t) = \Omega \tag{1}$$

where $\vec{r}$ is the position vector, $t$ is the time, $\vec{e}_i$ is the set of velocity vectors (See Fig. 1), that defines the lattice grid and over which the $f_i$ populations are distributed, $\Omega$ is the two-relaxation-time collision operator model (TRT) (Ginzburg and d'Humières, 2003; d'Humières and Ginzburg, 2009).

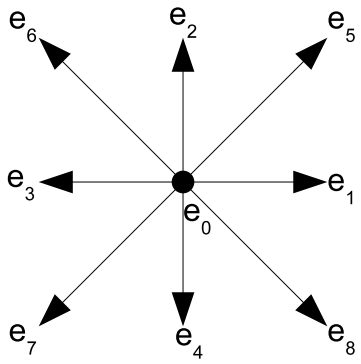


Figure 1: The 9 velocity vectors $\vec{e}_i$ of the lattice grid D2Q9.

It has one part named symmetric (superscript $+$) and another named anti-symmetric (superscript $-$) defined as,

$$\Omega = -\Omega^{+} - \Omega^{-} \tag{2}$$

$$\Omega^{\pm} = \omega^{\pm}\left[f_i^{\pm}(\vec{r}, t) - f_i^{eq,\pm}(\vec{r}, t)\right] \tag{3}$$

$$f_i^{\pm} = \frac{f_i(\vec{r}, t) \pm f_{\bar{i}}(\vec{r}, t)}{2} \tag{4}$$

$$f_i^{eq,\pm} = \frac{f_i^{eq}(\vec{r}, t) \pm f_{\bar{i}}^{eq}(\vec{r}, t)}{2} \tag{5}$$

where $f_i^{eq}$ is the discrete Maxwellian equilibrium distribution function, and the subscript $\bar{i}$ represents the opposite velocity vector of $i$, $\omega^{\pm}$ are the relaxation frequencies for the symmetrical and anti-symmetric parts. Herein, the relation between relaxation frequencies is

$$\omega^{-} = \frac{8(2-\omega^{+})}{8-\omega^{+}} \tag{6}$$

which guarantees good precision on boundaries and correct computations of fluxes between a wall and fluid nodes in the bounce-back scheme for non-slip wall boundary conditions. The discrete equilibrium distribution function can be written as,

$$f_i^{eq} = w_i \rho \left\{1 + 3\vec{e}_i \cdot \vec{u} + \frac{9(\vec{e}_i \cdot \vec{u})^2}{3} - \frac{3\vec{u}^2}{2}\right\} \tag{7}$$

where $w_i$ are the weighting factors: $w_0 = \frac{4}{9}$, $w_{1,2,3,4} = \frac{1}{9}$, and $w_{5,6,7,8} = \frac{1}{36}$, respectively to each microvelocity in a D2Q9 scheme, Fig. 1 employed in the present work.

The macroscopic density and velocity are moments of the distribution function. They are calculated through the following summations,

$$\rho = \sum_i f_i \tag{8}$$

$$\rho\,\vec{u} = \sum_i \vec{e}_i\, f_i \tag{9}$$

The Chapman-Enskog expansion of Eq. 1 determines the relation between the relaxation frequency and apparent kinematic viscosity (Ginzburg, 2005), and results in,

$$\nu_{app} = \left(\frac{1}{\omega^+} - \frac{1}{2}\right)\frac{1}{3}. \tag{10}$$

that is defined through the rheological model by

$$\nu_{app} = \frac{\tau}{\rho\dot{\gamma}} \tag{11}$$

For a non-Newtonian fluid with time-independent properties, the $\nu_{app}$ could be expressed depending on the local strain rate. The local strain-rate tensor $D_{\alpha,\beta}$ is defined as

$$D_{\alpha,\beta} = -\frac{\omega^+}{2\rho c_s^2}\sum_i e_{i,\alpha}e_{i,\beta}(f_i - f_i^{eq}), \tag{12}$$

where $\alpha$ and $\beta$ are the Cartesian coordinates. The strain-rate $\dot{\gamma}$ calculated by,

$$\dot{\gamma} = \sqrt{2\sum_{\alpha,\beta=1}^{2} D_{\alpha,\beta}D_{\alpha,\beta}} \tag{13}$$

In this work, we employ a fluid with power-law constitutive relation, which under simple shearing conditions is determined by Eq. 14:

$$\tau = k\dot{\gamma}^n \tag{14}$$

where $k$ is the consistency and $n$ is the flow index that gives the non-linearity between shear stress and shear strain rate. The system is then solved in the following sequence at every time step: (1) guess a value for $\omega^+$ and calculate Eq. 10 for apparent kinematic viscosity; (2) solve Eqs. 12 and 13 for strain-rate tensor and strain-rate; (3) calculate Eq. 14 for shear stress; (4) calculate Eq. 11; (5) compare the $\nu_{app}$ from step (1) to $\nu_{app}$ from step (4); (6) if greater than a tolerance value, then return to step (2). After this sequence, relax and propagate Eq. 1. The simulation is performed until convergence is reached.

### 2.1 Domain and Problem set-up

This section shows the domain, fluids parameters, and simulation criteria used. All the simulations were performed for steady-state laminar flow of Newtonian and shear thinning (pseudoplastic) fluids inside a horizontal channel with its lower half filled with porous media. Figure 2 shows the domain and the boundary conditions used.

The domain was set with D equal to 80 lattices and H equal to 1000 lattices. The periodic cell has $L$ = 40 lattices. Only ordered porous media were used with pore diameter $D_p$ equal to 10, 15, 20, 25, and 30 lattices. The flow periodic boundary conditions were used at the entrance and exit of the channel to simulate fully developed flows. The results were compared with a pure Hagen-Poiseuille flow in the upper half. The Reynold number was equal to 10 based on the upper free flow. A pressure gradient was imposed as a body force $F_b$ and set accordingly to the desired Reynolds number. Three fluids were set, two shear-thinning fluids with flow index $n$ equal to 0.50 and 0.75, and the Newtonian fluid ($n$ = 1.0). The consistency $k$ and viscosity $\nu$ was equal to $1/6$ by setting $\omega^+$ equal to 1.0.

## 3. RESULTS

From the numerical procedure, the velocity field $\vec{u}$ was obtained as the solution of interest for the problem at hand. Averaging both longitudinal ($u$) components in $x$-direction, the velocity profile $u(y)$ was obtained. Given the nature of the flow, the vertical $v$ component was not explored. A typical solution for $u(y)$ can be seen in Fig. 3 for $n$ = 0.50 and $D_p$ = 30.

From Fig. 3 it can be seen the classical flatten profile for $n < 1.00$ close to the center of the channel. Inside the porous wall $y < 1000$, the flow assumes preferable paths and present values much smaller than the free flow ($\sim 10^{-4}$).

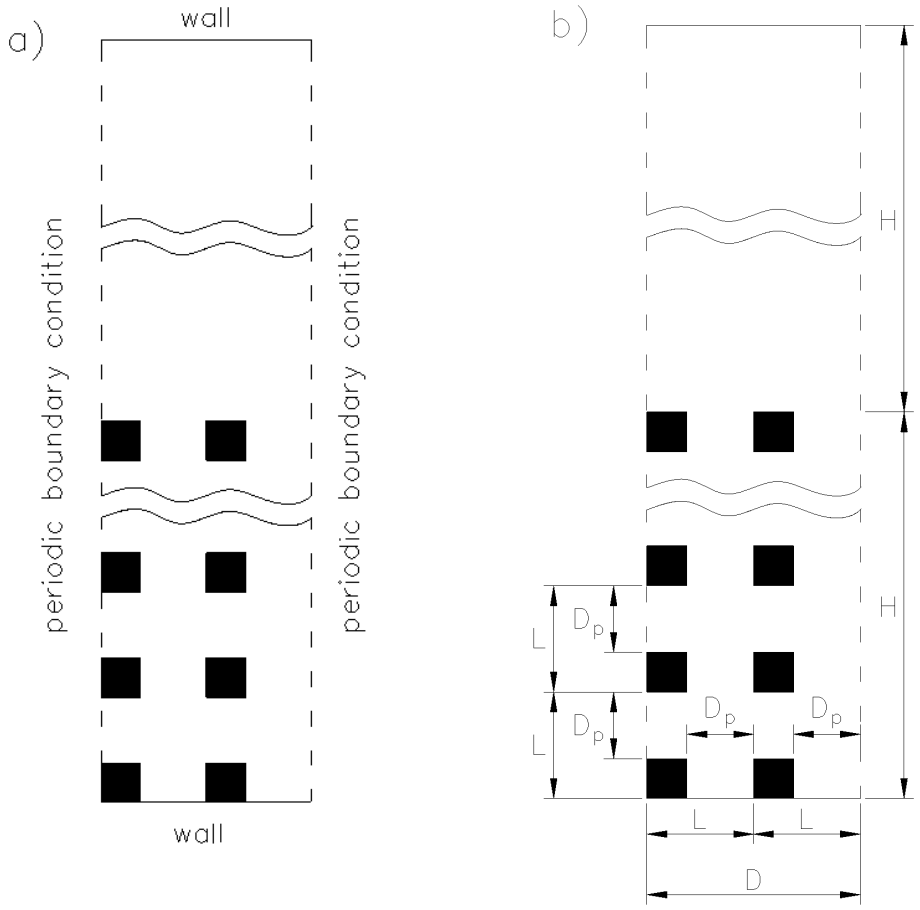


(a) Boundary Conditions (b) Dimensions

Figure 2: Schematic figures of the domain used on the simulations. a) Boundary conditions. b) Dimensions of the domain.

Another important feature of this solution is how the flow gains momentum as it leaves the porous medium. This can be used to stipulate boundary conditions for macroscopic solutions without need for solving the porous flow (as in Beavers and Joseph (1967), for example). Fig. 3 shows that, close to the interface between the porous flow and free flow, the longitudinal velocity greatly increases, two order of magnitude ($\sim 10^{-2}$) in comparison to the flow inside the porous domain.

To understand the general influence the parameters have over the the flow, the first main integral property that can be explored is the Darcian velocity, i.e. average flow velocity inside the porous medium, $u_{Darcy}$. To calculate such value, without considering its variation due to the interface and fixed wall (at $y = 0$), $u_{Darcy}$ was calculated as the average of $u(y)$ for $100 < y < 900$. This result is shown in Fig. 4.

For an increasing in pore diameter $D_p$ (than increase in porosity), all results show the expected behavior as $u_{Darcy}$ increases. With more void space to flow, less friction forces are offered, and greater velocities can be achieve for the same pressure gradient. Moreover, an interesting feature is rendered clear as $n$ assumes values of a shear thinning fluid ($n < 1.00$). For the same pressure gradient, $u_{Darcy}$ obtained values are smaller, showing that the hydraulic resistance offered by the porous matrix is greater when $n < 1.00$. This is a counter-intuitive response since, given a fixed $Re$, one would expect the apparent viscosity to be lower as $n$ is smaller.

Another interesting feature to observe is the derivative at the exact interface, where $y^* = 0$. To obtain such property, we interpolated the solution $u(y)$ using a cubic function and numerically calculated the derivative of $u(y)$ for the interpolated function using a second-order difference scheme. The results can be observed in Fig. 5

A quasi-linear behavior is observed for $\partial u/\partial y|_{y^*=0}$ as function of $D_p$. This result states, for instance, that relations such as Beavers and Joseph (1967) could be directly expressed as a function of the porosity/pore diameter. Moreover, such relation would be even valid for other types of shear-thinning fluids, rendering easier the solution for simplistic models of the free flow. Another observation that can be retained is the increase in the derivative as $n$ is smaller. This is corroborated by Fig. 4: as $u_{Darcy}$ is smaller for $n < 1.00$, a stronger gradient exists between free flow and porous flow, thus augmenting the derivative at the interface.

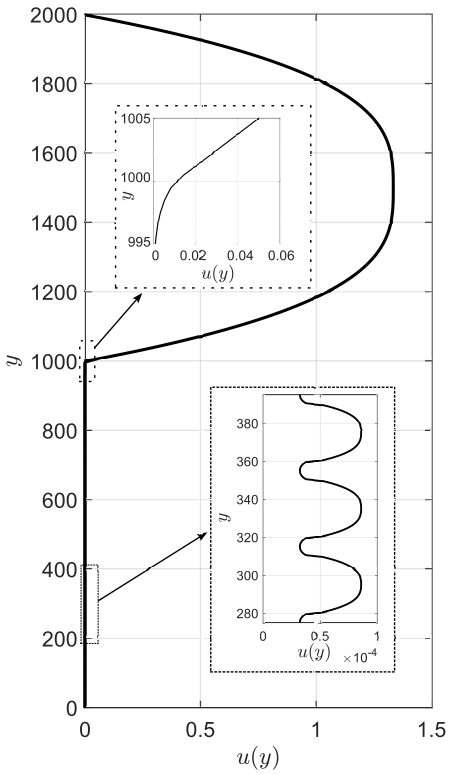


Figure 3: Typical solution for the velocity profile $u(y)$ for $n$ = 0.50 and $D_p$ = 30.

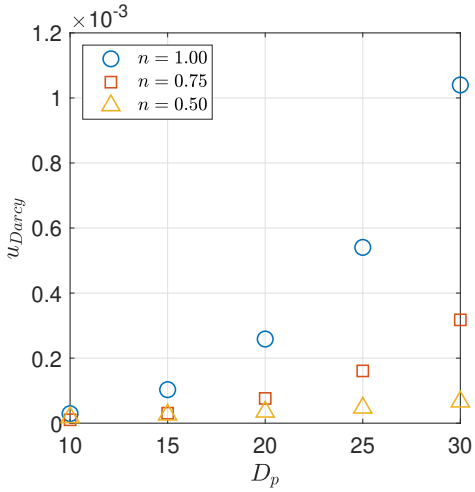


Figure 4: Darcian velocity as function of the pore diameter $D_p$ and flow index $n$.

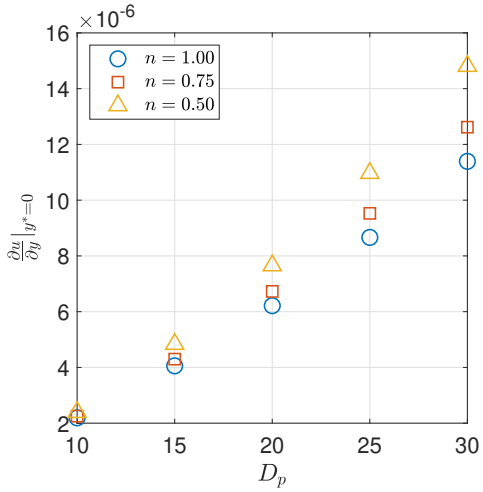


Figure 5: Derivative of the velocity profile $\partial u/\partial y|_{y^*=0}$ as function of the pore diameter $D_p$ and flow index $n$.

Finally, an integral property of interest to highlight is the discharge gain $\Delta q$, which is expressed as:

$$\Delta q = \int_{y^*=0}^{H} (u - u_{np}) dy \tag{15}$$

where $u_{np}$ is the solution for a plane Poiseuille flow of a shear thinning fluid (with $n \leq 1.00$). This property represent the increase in quantity of volume that can flow through the channel height $H$ when the channel is in contact with a porous wall filled with the same fluid. Figures 6 and 7 represent how such a quantity depend on the previously mentioned parameters $D_p$ and $u_{Darcy}$.

Once again, we can identify that for greater pore diameters $D_p$, the free flow would show a greater discharge gain, thus signifying a smaller head loss, as shown Fig. 6. However, the physical interface or boundary between the free flow

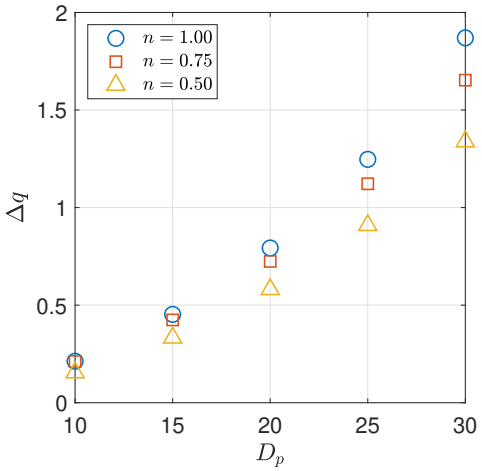


Figure 6: Gain of discharge $\Delta q$ as function of the pore diameter $D_p$ and flow index $n$.

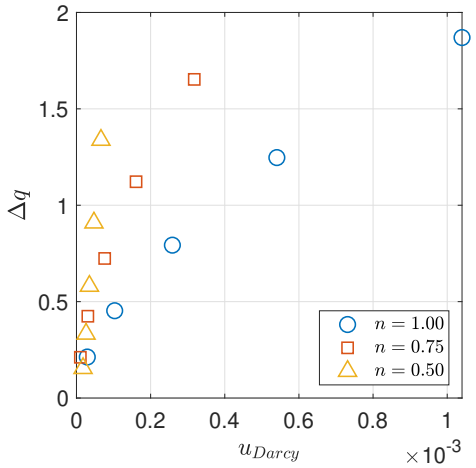


Figure 7: Gain of discharge $\Delta q$ as function of $u_{Darcy}$.

and porous flow dictates the head loss. Since for non-Newtonian fluids, the porous flow shows greater resistance, i.e. low values for $u_{Darcy}$ in the simulations here performed, one would expect that the interface velocity $u(y^* = 0)$ would be closer to zero, than to a velocity profile similar to $u_{np}$. This is somehow perceived as $\Delta q$ is relatively smaller for shear thinning fluids $n < 1.00$. Finally, an interesting feature arises when evidencing $\Delta q$ against $u_{Darcy}$, as shown Fig. 7. The gain in discharge is far greater for shear-thinning fluids for the same Darcian flow, reaching values up to 3 times greater than the data obtained in the simulations here performed.

## 4. CONCLUSIONS

This paper studied the non-Newtonian fluid flow in a half-filled porous channel. The Lattice Boltzmann Method was used to solve simultaneously the upper channel flow and bottom porous flow, without any simplifications or imposed boundary conditions at the interface. The results analyzed how the porous diameter $D_p$ and fluid index $n$ affects the Darcian velocity $u_{Darcy}$, the velocity derivative $\partial u/\partial y|_{y^*=0}$ at interface and discharge gain $\Delta q$

The main findings are:

- The value for longitudinal velocity inside the porous region is $\sim 10^{-4}$ while immediately after the porous interface, the flow gains momentum and it increases to $\sim 10^{-2}$.
- For the same pressure gradient,the values obtained for $u_{Darcy}$ are smaller, showing that the hydraulic resistance offered by the porous matrix is greater when $n < 1.00$.
- A quasi-linear behavior is observed for $\partial u/\partial y|_{y^*=0}$ as a function of $D_p$, which enforces that the conditions on the interface could be directly expressed as a function of the porosity/pore diameter.
- The $\Delta q$ is far greater for shear thinning fluids for the same Darcian flow, reaching values up to 3 times greater within the data obtained in the simulations here performed.

## 5. REFERENCES

Aharonov, E. and Rothman, D.H., 1993. "Non-Newtonian flow (through porous media): a lattice-Boltzmann method". *Geophysical Research Letters*, Vol. 20, No. 8, pp. 679–682.

Bars, M.L. and Worster, M.G., 2006. "Interfacial conditions between a pure fluid and a porous medium: implications for binary alloy solidification". *Journal of Fluid Mechanics*, Vol. 555, p. 149–173.

Beavers, G.S. and Joseph, D.D., 1967. "Boundary conditions at a naturally permeable wall". *Journal of Fluid Mechanics*, Vol. 30, pp. 197–207.

Cloete, M. and Smit, F., 2012. "Modeling of generalized newtonian fluid flow at a fluid-porous interface". *AIP Conference Proceedings*, Vol. 1479, No. 1, pp. 181–184.

d'Humières, D. and Ginzburg, I., 2009. "Viscosity independent numerical errors for lattice boltzmann models: From recurrence equations to "magic" collision numbers". *Computers and Mathematics with Applications*, Vol. 58, pp. 823–840.

Fiorot, G.H. and Maciel, G.D.F., 2019. "Free-surface laminar flow of a Herschel–Bulkley fluid over an inclined porous

bed". *Journal of Non-Newtonian Fluid Mechanics*, Vol. 272, No. September, p. 104164. ISSN 0377-0257. doi: 10.1016/j.jnnfm.2019.104164.

Ginzburg, I., 2005. "Equilibrium-type and link-type lattice Boltzmann models for generic advection and anisotropic-dispersion equation". *Advances in Water Resources*, Vol. 28, No. 11, pp. 1171–1195. ISSN 03091708. doi: 10.1016/j.advwatres.2005.03.004.

Ginzburg, I. and d'Humières, D., 2003. "Multireflection boundary conditions for lattice boltzmann models". *Phisical Review E*, Vol. 68, p. 066614.

Rakotomalala, N., Salin, D. and Watzky, P., 1996. "Simulations of viscous flows of complex fluids with a Bhatnagar, Gross, and Krook lattice gas". *Physics of Fluids*, Vol. 8, No. 11, pp. 3200–3202. ISSN 10706631. doi: 10.1063/1.869093.

Sengupta, S. and De, S., 2019. "Couette–poiseuille flow of a bingham fluid through a channel overlying a porous layer". *Journal of Non-Newtonian Fluid Mechanics ()*, Vol. 265, p. 28–40.

Sullivan, S.P., Gladden, L.F. and Johns, M.L., 2006. "Simulation of power-law fluid flow through porous media using lattice Boltzmann techniques". *Journal of Non-Newtonian Fluid Mechanics*, Vol. 133, No. 2-3, pp. 91–98. ISSN 03770257. doi:10.1016/j.jnnfm.2005.11.003.

## 6. RESPONSIBILITY NOTICE

The authors are solely responsible for the printed material included in this paper.